General Four-Component Scattering Power Decomposition with Unitary Transformation of Coherency Matrix

Gulab Singh, *Member, IEEE*, Yoshio Yamaguchi, *Fellow, IEEE* and Sang-Eun Park, *Member, IEEE*

***Abstract*—This paper presents a new general four-component scattering power decomposition method by implementing a set of unitary transformations for the polarimetric coherency matrix. There exist 9 real independent observation parameters in the 3 x 3 coherency matrix with respect to the second order statistics of polarimetric information. The proposed method accounts for all observation parameters in the new scheme. It is known that the existing four-component decomposition method reduces the number of observation parameters from 9 to 8 by rotation of the coherency matrix, and that it accounts for 6 parameters out of 8, leaving 2 parameters (i.e., real and imaginary part of T_{13} component) un-accounted for. By additional special unitary transformation to this rotated coherency matrix, it became possible to reduce the number of independent parameters from 8 to 7. After the unitary transformation, the new four-component decomposition is carried out that accounts for all parameters in the coherency matrix including the remaining T_{13} component. Therefore, the proposed method makes use of full utilization of polarimetric information in the decomposition.**

The decomposition also employs an extended volume scattering model, which discriminates the volume scattering between dipole and dihedral scattering structures caused by the cross-polarized *HV* component. It is found that the new method enhances the double bounce scattering contributions over the urban areas compared to those of the existing four-component decomposition, resulting from the full utilization of polarimetric information.

***Index Terms*—Radar polarimetry, scattering power decomposition, polarimetric synthetic aperture radar**

I. Introduction

SCATTERING power decompositions have been a research topic in radar polarimetry for the analysis of fully polarimetric synthetic aperture radar data [1]-[14]. There exist 9 real independent polarimetric parameters in the 3 x 3 coherency or covariance matrices [2]. Physical model-based scattering power decomposition tries to account for these polarimetric parameters as much as possible in the decomposition. The original 3-component decomposition was proposed by Freeman and Durden [3] under the reflection symmetry condition that the cross-correlation between the co- and cross-polarized scattering elements are close to zero for natural distributed objects. This method accounts for 5 terms out of 9 independent parameters. In order to accommodate the decomposition scheme for more general scattering cases encountered in urban areas or by more complicated geometric scattering structures, Yamaguchi *et al*. [4] have added a helix scattering term and proposed the four-component decomposition. This helix power is generated by the imaginary part of $T_{23} = \left\langle \left(S_{HH} - S_{VV}\right) S_{HV}^{*} \right\rangle$ in the coherency matrix [5], and the related method accounts for 6 parameters out of 9, leaving 3 un-accounted. Then, by using the rotation of coherency matrix, An *et al*. [6], Lee and Ainsworth [1] and Yamaguchi *et al*. [7] reduced the number of polarization parameter from 9 to 8. These methods yielded better decomposition results by accounting for 6 parameters out of 8 [8]. The un-accounted parameters are the real and imaginary part of $T_{13} = \left\langle \left(S_{HH} + S_{VV}\right) S_{HV}^{*} \right\rangle$ in the coherency matrix. They still remain un-accounted in any of the known physical scattering model-based decompositions [1]-[8].

In this paper, a new general four-component decomposition method is proposed using a special unitary transformation to the rotated coherency matrix, which has been used in the existing four-component decomposition [7]. Since unitary transformations do not change any information included in the coherency matrix, the rotated coherency matrix is transformed by a special unitary transformation to eliminate the T_{23} element. The new features are the reduction in the number of observed polarization parameters from 8 to 7, and accounting for the remaining T_{13} element. This new four-component decomposition finally accounts for 7 terms out of 7 polarimetric parameters. It is shown that this method yields accurate and/or similar decomposed images compared with those by the existing four-component decomposition [7], [8].

In section II, a basic principle for reduction of polarization parameters is explained by implementing the unitary transformation for the coherency matrix. Based on the unitary transformation of the rotated coherency matrix, a new 4-component scattering power decomposition scheme is carried out in section III. At this decomposition stage, all elements of the coherency matrix are utilized to derive four-component scattering powers, i.e., surface, double bounce, volume, and helix scattering powers. An extended volume

Manuscript received September 22, 2011; revised March 12, 2012; revised May 28, 2012; accepted July 23, 2012. This work was supported in part by the Ministry of Education, Japan under the Space Sensing Project Grant at Niigata University.

Authors are with the Graduate School of Science and Technology, Niigata University, Niigata, 950-2181, Japan, (phone/fax: +81-25-262-6752 e-mail: g.singh@wave.ie.niigata-u.ac.jp).

scattering model is also incorporated to discriminate against the volume scattering between dipole and dihedral scatterings caused by the cross-polarized *HV* component [8]. Section IV shows some decomposition results in comparison with the existing 4-component scattering power decomposition. A conclusion is given in Section V.

II. Basic Principle For Double Unitary Transformation

By acquiring the scattering matrix data sets, the corresponding coherency matrix can be recovered, which retains the second order statistics of polarimetric information. The ensemble average of the coherency matrix is given as

$$\langle [T] \rangle = \left\langle \boldsymbol{k}_p \boldsymbol{k}_p^{\dagger} \right\rangle = \begin{bmatrix} T_{11} & T_{12} & T_{13} \\ T_{21} & T_{22} & T_{23} \\ T_{31} & T_{32} & T_{33} \end{bmatrix} \tag{1}$$

where † denotes complex conjugation and transpose, < > denotes ensemble average, and the Pauli vector $\boldsymbol{k}_p$ is defined as

$$\boldsymbol{k}_p = \frac{1}{\sqrt{2}} \begin{bmatrix} S_{HH} + S_{VV} \\ S_{HH} - S_{VV} \\ 2\, S_{HV} \end{bmatrix} \tag{2}$$

There are 9 independent and real-valued polarization parameters included in the general form of the coherency matrix (1).

Unitary transformation preserves all information contained in the 3 x 3 positive definite coherency matrices without loss of generality. This guarantees that observed polarimetric information remains in the coherency matrix after unitary transformation. Using this mathematical property, it is possible to transform the measured coherency matrix (1) to a new one with $T_{23} = 0$ as

$$\langle [T'] \rangle = \begin{bmatrix} T'_{11} & T'_{12} & T'_{13} \\ T'_{21} & T'_{22} & 0 \\ T'_{31} & 0 & T'_{33} \end{bmatrix} . \tag{3}$$

If the T_{23} element is eliminated, the number of independent information in the coherency matrix becomes 7, for which new scattering power decomposition is carried out. The reason why we choose T_{23} element is that the helix scattering is directly related to this term. In order to achieve $T_{23} = 0$, the unitary transformation is implemented twice.

The first one is the rotation of around radar line of sight [7]

$$\langle [T(\theta)] \rangle = [R(\theta)] \langle [T] \rangle [R(\theta)]^{\dagger} \tag{4}$$

with a unitary rotation matrix,

$$[R(\theta)] = \begin{bmatrix} 1 & 0 & 0 \\ 0 & \cos 2\theta & \sin 2\theta \\ 0 & -\sin 2\theta & \cos 2\theta \end{bmatrix} . \tag{5}$$

The angle θ is chosen as to minimize the T_{33} element [7]

$$2\theta = \frac{1}{2} \tan^{-1} \left(\frac{2 \operatorname{Re} \{T_{23}\}}{T_{22} - T_{33}} \right) . \tag{6}$$

After this rotation, the T_{23} element becomes purely imaginary,

$$T_{23}(\theta) = j \operatorname{Im} (T_{23}) . \tag{7}$$

Then, the second unitary transformation is employed such that

$$\langle [T(\varphi)] \rangle = [U(\varphi)] \langle [T(\theta)] \rangle [U(\varphi)]^{\dagger} \tag{8}$$

with a special unitary transform matrix,

$$[U(\varphi)] = \begin{bmatrix} 1 & 0 & 0 \\ 0 & \cos 2\varphi & j \sin 2\varphi \\ 0 & j \sin 2\varphi & \cos 2\varphi \end{bmatrix} \tag{9}$$

The angle φ is derived so as to minimize the T_{33} element in a way similar to [7]

$$2\varphi = \frac{1}{2} \tan^{-1} \left(\frac{2 \operatorname{Im} \{T_{23}(\theta)\}}{T_{22}(\theta) - T_{33}(\theta)} \right) \tag{10}$$

This unitary transformation yields the coherency matrix element as

$$\begin{aligned} T_{11}(\varphi) &= T_{11}(\theta) = T_{11} \\ T_{12}(\varphi) &= T_{21}^{*}(\varphi) = T_{12}(\theta) \cos 2\varphi - j\, T_{13}(\theta) \sin 2\varphi \\ T_{13}(\varphi) &= T_{31}^{*}(\varphi) = T_{13}(\theta) \cos 2\varphi - j\, T_{12}(\theta) \sin 2\varphi \\ T_{22}(\varphi) &= T_{22}(\theta) \cos^2 2\varphi + T_{33}(\theta) \sin^2 2\varphi + \operatorname{Im}\{T_{23}(\theta)\} \sin 4\varphi \\ T_{23}(\varphi) &= T_{32}^{*}(\varphi) = \operatorname{Re} \{T_{23}(\theta)\} \\ T_{33}(\varphi) &= T_{33}(\theta) \cos^2 2\varphi + T_{22}(\theta) \sin^2 2\varphi - \operatorname{Im}\{T_{23}(\theta)\} \sin 4\varphi \end{aligned} \tag{11}$$

This second unitary transformation forces the T_{23} element to be zero using (11) and (7).

$$T_{23}(\varphi) = \operatorname{Re} \{T_{23}(\theta)\} = \operatorname{Re} \{ j \operatorname{Im} (T_{23}) \} = 0 \tag{12}$$

Hence, the T_{23} element is completely eliminated as shown in (12). Therefore, it can be theoretically reduced the number of independent polarization parameters from 9 to 7 by unitary transform twice as shown in (3).

It should be noted that the T_{13} element still remains as a complex number, which has not been incorporated in any physical model-based decomposition.

III. New Four-Component Scattering Power Decomposition

In this section, a new four-component scattering power decomposition is presented using (8). The four-component powers represent surface scattering power P_s, double bounce scattering power P_d, volume scattering power P_v and helix scattering power P_c. Illustrative examples for these powers are shown in Fig. 1 which are well known from the pertinent literature [1]-[9].

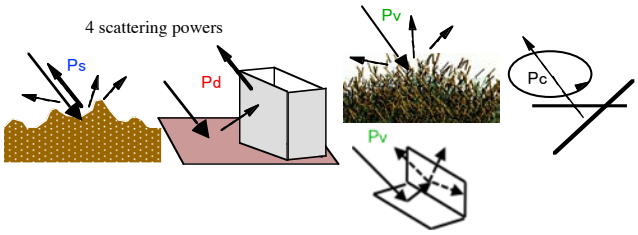

Fig. 1. Illustrative examples of four-component scattering powers: surface scattering power P_s, double bounce scattering power P_d, volume scattering power P_v and helix scattering power P_c.

The starting point is the 4-component decomposition after the rotation (4), expressed as

$$\langle [T(\theta)] \rangle = f_s \langle [T] \rangle_{surface} + f_d \langle [T] \rangle_{double} + f_v \langle [T] \rangle_{vol} + f_c \langle [T] \rangle_{helix} \tag{13}$$

where f_s, f_d, f_v and f_c are expansion coefficients to be determined, and the four sub-matrices represent physical scattering models in the form of coherency matrix description [7], [8]. The details are given in reference [7]. In this expression, 6 terms out of 8 parameters are accounted for, for which the un-accounted 2 terms are real and imaginary parts of T_{13}. Now we transform (13) using unitary transformation (8) so that the T_{13} element can be accounted for. The model expansion can be transformed from the rotated basis to the new unitary basis such that

$$\langle [T(\varphi)] \rangle = [U(\varphi)]$$

$$\left(f_s \langle [T] \rangle_{surface} + f_d \langle [T] \rangle_{double} + f_v \langle [T] \rangle_{vol} + f_c \langle [T] \rangle_{helix} \right) [U(\varphi)]^{\dagger}$$

$$= f_s \langle [T(\varphi)] \rangle_{surface} + f_d \langle [T(\varphi)] \rangle_{double} + f_v \langle [T(\varphi)] \rangle_{vol} + f_c \langle [T(\varphi)] \rangle_{helix} \tag{14}$$

The expansion matrices on the right hand side of (14) after unitary transformation become as derived in detail next:

A. Theoretical expansion matrices for scattering models

The expansion matrix for surface scattering is expressed as

$$\langle [T(\varphi)] \rangle_{surface} = [U(\varphi)] \langle [T] \rangle_{surface} [U(\varphi)]^{\dagger}$$

$$= [U(\varphi)] \begin{bmatrix} 1 & \beta^* & 0 \\ \beta & |\beta|^2 & 0 \\ 0 & 0 & 0 \end{bmatrix} [U(\varphi)]^{\dagger}$$

$$= \begin{bmatrix} 1 & \beta^* \cos 2\varphi & -j\beta^* \sin 2\varphi \\ \beta \cos 2\varphi & |\beta|^2 \cos^2 2\varphi & -j|\beta|^2 \dfrac{\sin 4\varphi}{2} \\ j\beta \sin 2\varphi & j|\beta|^2 \dfrac{\sin 4\varphi}{2} & |\beta|^2 \sin^2 2\varphi \end{bmatrix} \tag{15}$$

The double bounce scattering model is defined as

$$\langle [T(\varphi)] \rangle_{double} = [U(\varphi)] \langle [T] \rangle_{double} [U(\varphi)]^{\dagger}$$

$$= [U(\varphi)] \begin{bmatrix} |\alpha|^2 & \alpha & 0 \\ \alpha^* & 1 & 0 \\ 0 & 0 & 0 \end{bmatrix} [U(\varphi)]^{\dagger}$$

$$= \begin{bmatrix} |\alpha|^2 & \alpha \cos 2\varphi & -j\alpha \sin 2\varphi \\ \alpha^* \cos 2\varphi & \cos^2 2\varphi & -j \dfrac{\sin 4\varphi}{2} \\ j\alpha^* \sin 2\varphi & j \dfrac{\sin 4\varphi}{2} & \sin^2 2\varphi \end{bmatrix} \tag{16}$$

The helix scattering model is written as

$$\langle [T(\varphi)] \rangle_{helix} = [U(\varphi)] \langle [T] \rangle_{helix} [U(\varphi)]^{\dagger}$$

$$= [U(\varphi)] \frac{1}{2} \begin{bmatrix} 0 & 0 & 0 \\ 0 & 1 & \pm j \\ 0 & \mp j & 1 \end{bmatrix} [U(\varphi)]^{\dagger}$$

$$= \frac{1}{2} \begin{bmatrix} 0 & 0 & 0 \\ 0 & 1 \pm \sin 4\varphi & \pm j \cos 4\varphi \\ 0 & \mp j \cos 4\varphi & 1 \mp \sin 4\varphi \end{bmatrix} \tag{17}$$

B. Four-component Decomposition Depending on the Volume Scattering Model

Since there are 4 scattering models [8] for volume scattering, according to the generation of the cross-polarized *HV* term, the decomposition scheme is applied accordingly. For volume scattering caused by the *HV* component by vegetation, one of the following distributions is chosen based on the magnitude balance of $|S_{HH}|^2$ and $|S_{VV}|^2$ [8], i.e., 1) uniform distribution, 2) cosine distribution, or 3) sin distribution.

1) Uniform distribution: $p(\theta) = \dfrac{1}{2\pi}$

$$\langle [T(\varphi)] \rangle_{vol} = [U(\varphi)] \frac{1}{4} \begin{bmatrix} 2 & 0 & 0 \\ 0 & 1 & 0 \\ 0 & 0 & 1 \end{bmatrix} [U(\varphi)]^{\dagger} = \frac{1}{4} \begin{bmatrix} 2 & 0 & 0 \\ 0 & 1 & 0 \\ 0 & 0 & 1 \end{bmatrix} \tag{18}$$

The element relations after the unitary transformation (14) are expanded. The expansion of (14) leads to the following relations,

$$\begin{aligned} T_{11}' &= f_s + f_d |\alpha|^2 + \frac{1}{2} f_v \\ T_{22}' &= \left(f_s |\beta|^2 + f_d \right) \cos^2 2\varphi + \frac{1}{4} f_v + \frac{1}{2} f_c \left(1 \pm \sin 4\varphi \right) \\ T_{33}' &= \left(f_s |\beta|^2 + f_d \right) \sin^2 2\varphi + \frac{1}{4} f_v + \frac{1}{2} f_c \left(1 \mp \sin 4\varphi \right) \\ T_{12}' &= \left(f_s \beta^* + f_d \alpha \right) \cos 2\varphi \\ T_{13}' &= -j \left(f_s \beta^* + f_d \alpha \right) \sin 2\varphi \\ T_{23}' &= -\left(f_s |\beta|^2 + f_d \right) \sin 4\varphi \pm f_c \cos 4\varphi = 0 \end{aligned} \tag{19}$$

Arrangement of the element relations provides 5 equations with 6 unknowns (α, β, f_s, f_d, f_v, *and* f_c)

$$T_{11}' = f_s + f_d |\alpha|^2 + \frac{1}{2} f_v \tag{20}$$

$$T_{22}' + T_{33}' = f_s |\beta|^2 + f_d + \frac{1}{2} f_v + f_c \tag{21}$$

$$T_{22}^{'} - T_{33}^{'} = \left(f_s |\beta|^2 + f_d \right) \cos 4\varphi \pm f_c \sin 4\varphi \tag{22}$$

$$\begin{aligned} T_{12}^{'} + T_{13}^{'} &= \left(f_s \beta^* + f_d \alpha \right) \left(\cos 2\varphi - j \sin 2\varphi \right) \\ &= \left(f_s \beta^* + f_d \alpha \right) e^{-j 2\varphi} \end{aligned} \tag{23}$$

$$\left(f_s |\beta|^2 + f_d \right) \sin 4\varphi = \pm f_c \cos 4\varphi \tag{24}$$

From (24) and (22) together with (11) and (21), f_c and f_v, and the corresponding powers *Pc* and *Pv* can be derived

$$\begin{aligned} f_c = P_c &= \left| \left(T_{22}^{'} - T_{33}^{'} \right) \sin 4\varphi \right| \\ &= 2 \left| \mathrm{Im} \{ T_{23}(\theta) \} \right| = 2 \left| \mathrm{Im} \{ T_{23} \} \right| \end{aligned} \tag{25}$$

$$\begin{aligned} f_v = P_v &= 2 \left[\left(T_{22}^{'} + T_{33}^{'} \right) - \left(T_{22}^{'} - T_{33}^{'} \right) \cos 4\varphi - f_c \right] \\ &= 2 \left[2\, T_{33}(\theta) - f_c \right] \end{aligned} \tag{26}$$

Once f_c and f_v are determined, we have a set of 3 equations with 4 unknowns (α, β, f_s, *and* f_d)

$$\begin{cases} f_s + f_d |\alpha|^2 = S \\ f_s |\beta|^2 + f_d = D \\ f_s \beta^* + f_d \alpha = C \end{cases} \tag{27}$$

where

$$\begin{cases} S = T_{11}^{'} - \frac{1}{2} f_v \\ D = T_{22}^{'} + T_{33}^{'} - \frac{1}{2} f_v - f_c \\ C = \left(T_{12}^{'} + T_{13}^{'} \right) e^{j 2\varphi} \end{cases} \tag{28a}$$

(28a) can be further simplified using (11) as

$$\begin{cases} S = T_{11}(\theta) - \frac{1}{2} P_v \\ D = T_{22}(\theta) + T_{33}(\theta) - \frac{1}{2} P_v - P_c \\ C = T_{12}(\theta) + T_{13}(\theta) \end{cases} \tag{28b}$$

or

$$\begin{cases} S = T_{11} - \frac{1}{2} P_v \\ D = TP - P_v - P_c - S \\ C = T_{12}(\theta) + T_{13}(\theta) \end{cases} \tag{28c}$$

where *TP* is the total power.

2) Cosine distribution: $p(\theta) = \frac{1}{2} \cos \theta$

$$\begin{aligned} \langle [T(\varphi)] \rangle_{vol} &= [U_2(\varphi)] \frac{1}{30} \begin{bmatrix} 15 & -5 & 0 \\ -5 & 7 & 0 \\ 0 & 0 & 8 \end{bmatrix} [U_2(\varphi)]^{\dagger} \\ &= \frac{1}{30} \begin{bmatrix} 15 & -5 \cos 2\varphi & j 5 \sin 2\varphi \\ -5 \cos 2\varphi & 7 + \sin^2 2\varphi & j \dfrac{\sin 4\varphi}{2} \\ -j 5 \sin 2\varphi & -j \dfrac{\sin 4\varphi}{2} & 7 + \cos^2 2\varphi \end{bmatrix} \end{aligned} \tag{29}$$

The expression (14) is expanded in the same way as in 1) uniform distribution. After the expansion and rearrangement, a similar set of 3 equations with 4 unknowns can be obtained.

$$\begin{cases} f_s + f_d |\alpha|^2 = S \\ f_s |\beta|^2 + f_d = D \\ f_s \beta^* + f_d \alpha = C \end{cases} \tag{30}$$

where

$$\begin{cases} S = T_{11} - \frac{1}{2} P_v \\ D = TP - P_v - P_c - S \\ C = T_{12}(\theta) + T_{13}(\theta) + \frac{1}{6} P_v \end{cases} \tag{31}$$

and

$$\begin{cases} f_c = P_c = 2 \left| \mathrm{Im} \{ T_{23} \} \right| \\ f_v = P_v = \frac{15}{8} \left[2\, T_{33}(\theta) - f_c \right] \end{cases} \tag{32}$$

3) Sin distribution: $p(\theta) = \frac{1}{2} \sin \theta$

$$\begin{aligned} \langle [T(\varphi)] \rangle_{vol} &= [U(\varphi)] \frac{1}{30} \begin{bmatrix} 15 & 5 & 0 \\ 5 & 7 & 0 \\ 0 & 0 & 8 \end{bmatrix} [U(\varphi)]^{\dagger} \\ &= \frac{1}{30} \begin{bmatrix} 15 & 5 \cos 2\varphi & -j 5 \sin 2\varphi \\ 5 \cos 2\varphi & 7 + \sin^2 2\varphi & j \dfrac{\sin 4\varphi}{2} \\ j 5 \sin 2\varphi & -j \dfrac{\sin 4\varphi}{2} & 7 + \cos^2 2\varphi \end{bmatrix} \end{aligned} \tag{33}$$

After a similar expansion of (14) and rearrangement, it can be obtained a similar set of 3 equations with 4 unknowns.

$$\begin{cases} f_s + f_d |\alpha|^2 = S \\ f_s |\beta|^2 + f_d = D \\ f_s \beta^* + f_d \alpha = C \end{cases} \tag{34}$$

where

$$\begin{cases} S = T_{11} - \frac{1}{2} P_v \\ D = TP - P_v - P_c - S \\ C = T_{12}(\theta) + T_{13}(\theta) - \frac{1}{6} P_v \end{cases} \tag{35}$$

and

$$\begin{cases} f_c = P_c = 2 \left| \mathrm{Im} \{ T_{23} \} \right| \\ f_v = P_v = \frac{15}{8} \left[2\, T_{33}(\theta) - f_c \right] \end{cases} \tag{36}$$

4) For volume scattering caused by oriented dihedral scatter:

The following matrix is used [8],

$$\langle [T(\varphi)] \rangle_{vol} = [U(\varphi)] \frac{1}{15} \begin{bmatrix} 0 & 0 & 0 \\ 0 & 7 & 0 \\ 0 & 0 & 8 \end{bmatrix} [U(\varphi)]^{\dagger}$$

$$= \frac{1}{15}\begin{bmatrix} 0 & 0 & 0 \\ 0 & 7+\sin^2 2\varphi & j\dfrac{\sin 4\varphi}{2} \\ 0 & -j\dfrac{\sin 4\varphi}{2} & 7+\cos^2 2\varphi \end{bmatrix} \quad (37)$$

After the expansion (14) and rearrangement, a set of 3 equations with 4 unknowns can be obtained.

$$\begin{cases} f_s + f_d |\alpha|^2 = S \\ f_s |\beta|^2 + f_d = D \\ f_s \beta^* + f_d \alpha = C \end{cases} \quad (38)$$

where

$$\begin{cases} S = T_{11} \\ D = TP - P_v - P_c - S \\ C = T_{12}(\theta) + T_{13}(\theta) \end{cases} \quad (39)$$

and

$$\begin{cases} f_c = P_c = 2\,|\,\mathrm{Im}\,(T_{23})\,| \\ f_v = P_v = \dfrac{15}{16}\left[2\,T_{33}(\theta) - f_c\right] \end{cases} \quad (40)$$

C. Procedure to Solve 3 Equations with 4 Unknowns

The same set of three equations with 4 unknowns is obtained in (27), (30), and (34), respectively. In order to solve these equations, the same assumption [3]-[5] is used to eliminate one of the unknowns. Since the volume scattering coefficient f_v and the helix scattering coefficient f_c are obtained, the remaining dominant scattering mechanism (surface scattering or double bounce scattering) can be checked. The dominant scattering can be discriminated by the expansion of the C_{13} component for randomly distributed dipoles in the covariance matrix formulation [4].

$$\mathrm{Re}\left\{f_s \beta + f_d \alpha^*\right\} + \frac{1}{8} f_v - \frac{1}{4} f_c = \mathrm{Re}\left\{\left\langle S_{HH} S_{VV}^* \right\rangle\right\} \quad (41)$$

This equation can be re-arranged to

$$\begin{aligned} C_0 &= 2\,\mathrm{Re}\left\{f_s \beta + f_d \alpha^*\right\} \\ &= 2\,\mathrm{Re}\left\{S_{HH} S_{VV}^*\right\} - \frac{1}{4} f_v + \frac{1}{2} f_c \\ &= T_{11}^{'} - T_{22}^{'} - T_{33}^{'} + P_c \\ &= 2T_{11} - TP + P_c \end{aligned} \quad (42)$$

The sign of C_0 determines the dominant scattering mechanism, i.e., surface *versus* double bounce scattering.

If $C_0 > 0$, it can be assumed that the surface scattering is dominant. Since the double bounce scattering magnitude is negligible in this case, it can be assumed $|\alpha| << 1$ and fixed $\alpha = 0$. This condition leads to

$$f_s = S, \quad \beta^* = \frac{C}{S}, \quad f_d = D - \frac{|C|^2}{S} \quad (43)$$

If $C_0 \le 0$, it can be assumed that the double bounce scattering is dominant. Since the surface scattering magnitude is negligible in this case, it can be assumed $|\beta| << 1$ and putted $\beta^* = 0$. This condition leads to

$$f_d = D, \quad \alpha = \frac{C}{D}, \quad f_s = S - \frac{|C|^2}{D} \quad (44)$$

Once these coefficients are determined, the scattering powers can be derived from

$$P_s = f_s\left(1 + |\beta|^2\right) \quad (45)$$

$$P_d = f_d\left(1 + |\alpha|^2\right) \quad (46)$$

$$P_v = f_v \quad (47)$$

$$P_c = f_c \quad (48)$$

The equation (38) is solved with assumptions that the double bounce scattering is dominant so that the solution of (38) will be similar to the one of (44).

D. Decomposition Algorithm Implementation

The procedures in Sections II and III are summarized for implementation to POLSAR image analysis directly. The corresponding flow-chart of the new 4-component scattering power decomposition algorithm is shown in Fig. 2. In the first stage before the decomposition, the measured coherency matrix is rotated about the line of sight [10], and then a unitary transformation is applied on the rotated coherency matrix to force $T_{23} = 0$ for various scattering model expressions. It should be noted that arctan2 should be used for obtaining (6) and (10) in the computer algorithm. The number of independent parameters in the coherency matrix is reduced from 8 to 7 by the unitary transformation. The decomposition starts by retrieving the helix scattering power at this stage. Then the sign of a branch condition C_1 is checked for assigning the *HV* component. The condition is specifically developed for retrieving the *HV* component by dihedral scattering only in a similar way to (41) with (40),

$$\mathrm{Re}\left(f_s \beta + f_d \alpha^*\right) - \frac{7}{30} f_v - \frac{1}{4} f_c = \mathrm{Re}\left(S_{HH} S_{VV}^*\right) \quad (49)$$

$$\begin{aligned} C_1 &= 2\,\mathrm{Re}\left(f_s \beta + f_d \alpha^*\right) \\ &= 2\,\mathrm{Re}\left(S_{HH} S_{VV}^*\right) + \frac{7}{15} P_v + \frac{1}{2} P_c \\ &= T_{11}(\theta) - T_{22}(\theta) + \frac{7}{8} T_{33}(\theta) + \frac{1}{16} P_c \end{aligned} \quad (50)$$

Once assigned to the double scattering ($C_1 \le 0$), the dihedral expansion matrix (37) is used for the volume scattering. On other hand, if the surface scattering is assigned ($C_1 > 0$), one of the expansion matrices (18), (29) or (33) is used for the volume scattering based on the magnitude balance of $\left\langle |S_{HH}|^2 \right\rangle$ and $\left\langle |S_{VV}|^2 \right\rangle$. After determination of the volume scattering power, it is possible to determine the dominant scattering mechanism (surface *versus* double bounce) within the volume scattering by dipole scattering. Then four

scattering powers are obtained using C_0 of (42). This new decomposition accounts for inclusion of the all elements of the coherency matrix.

IV. Decomposition Results

In order to compare the results by this advanced method, two existing methods [7], [8] are examined for scattering

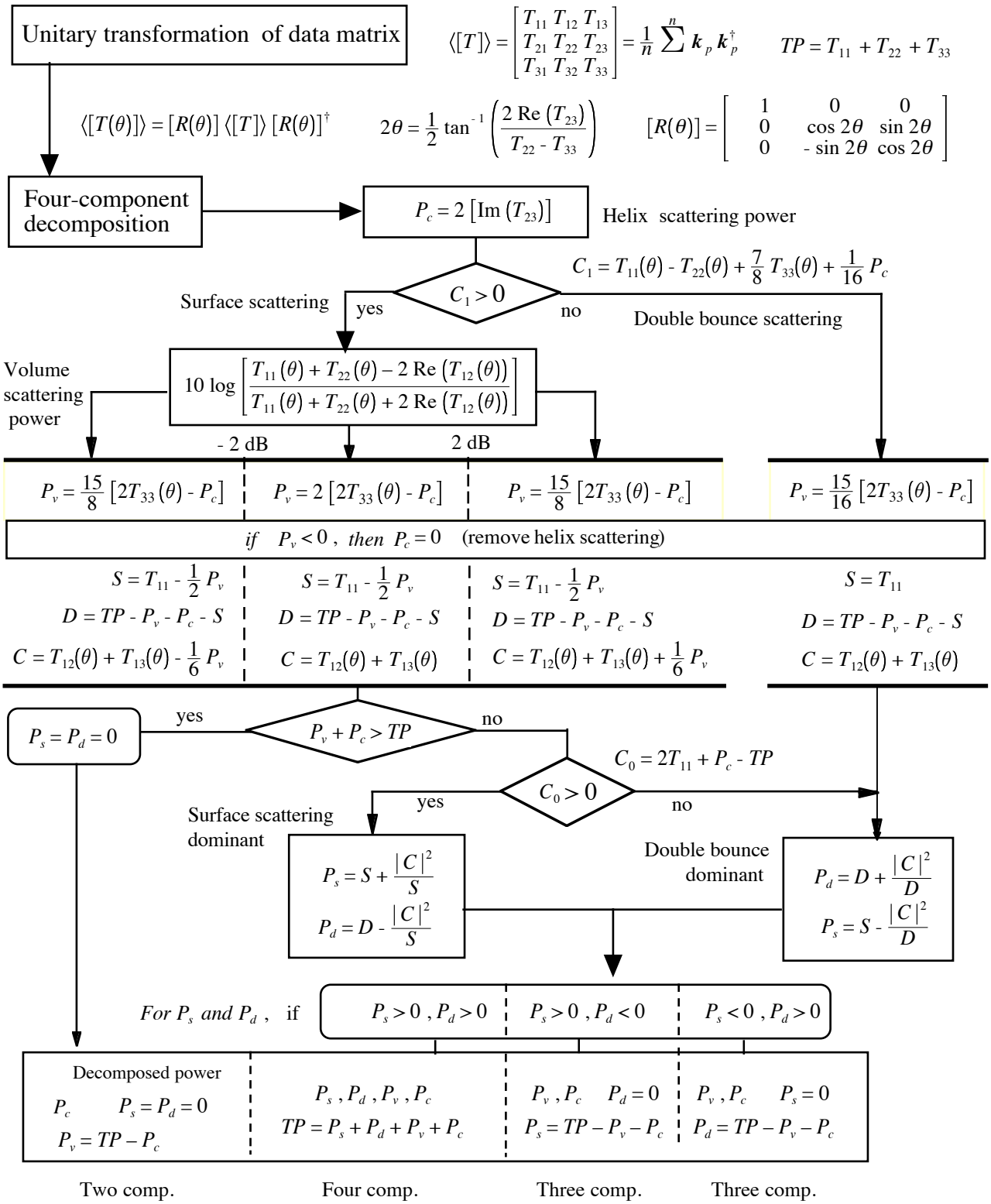

Fig. 2. Flow-chart of new four-component scattering power decomposition. All calculations can be executed from the elements of coherency matrix.

power decomposition, namely,

Y4R: 4-component decomposition with rotation of coherency matrix [7] which makes Re{T_{23}}=0. This method minimizes the cross-pol (T_{33}) scattering power generated by dipole scattering.

S4R: 4-component decomposition with rotation of coherency matrix [8] which makes Re{T_{23}}=0. This method minimizes the cross-pol (T_{33}) scattering power generated by dipole scattering plus dihedral scattering. One modification is made before applying to POLSAR data as compared to [8]. This modification is made in branch condition C_1 for selecting the dihedral volume scattering model. The modified C_1 is the same as proposed one in previous section III, while C_1 in [8] is $T_{11}(\theta) - T_{22}(\theta) - (1/2)\,P_c$. The modified C_1 is employed only for the purpose of retrieving dihedral scattering and of preserving volume scattering power in vegetation areas.

G4U: General 4-component decomposition (the present method) which makes T_{23}=0 by unitary transformation of $[T(\theta)]$. This method also minimizes the cross-pol (T_{33}) scattering power generated by dipole plus dihedral scattering.

These decomposition schemes are applied to many ALOS-PALSAR quad-pol. single look complex level 1.1 images for verifying the correct implementation of this scheme. For example, color-coded images over heterogeneous areas in San Francisco images are displayed in Fig. 3 using ALOS-PALSAR quad- pol data sets (Scene ID: ALPSRP276160750, acquired on April 1, 2011). The resolution is 30 m in the range and 5 m in the azimuth directions, respectively. The window size for the ensemble average in image processing was chosen as 2 in the range direction and 12 in the azimuth direction, which corresponds to 60 m by 60 m on the ground area. Results of the method derived in [7] and [8] are compared with the proposed method. It is seen that the double bounce scattering power P_d (Red) is either enhanced or kept similar in Fig. 3(a) as compared with Figs. 3(b) and 3(c) over the urban areas and man-made structures. It is also noticed that the surface scattering P_s (blue) is either enhanced or kept similar by the G4U as compared to the S4R and the Y4R over the vegetation area and sloped surface areas.

The close-up view of white rectangular areas on Fig. 3 is shown in Fig. 4. The interesting observation relates to the 40 degree oriented urban area in patch A on Fig. 4. The red color of the oriented urban area is enhanced in Fig. 4(a) as compared to 4(b) and 4(c). This enhancement of Red serves to recognize man-made structures from vegetation areas more easily. This is because the unitary transformation based method is accounting for all elements of the coherency matrix.

The decomposition power contribution of highly oriented dense urban areas in the San Francisco image are also shown in Table I, for patch A (black line box in Fig. 4) in San Francisco images in Fig. 4, for quantitative comparison of the existing 4-component schemes *versus* the proposed 4-component scheme. It can be seen that the volume scattering components of the methods G4U and S4R are decreased and the surface scattering components of the methods G4U and S4R are increased as compared to the method Y4R [7]. The double bounce scattering components of present methods are increased as compared to the methods Y4R [7] and S4R. The helix power remains invariant, which implies that the proposed method works well in highly oriented urban areas as compared to the existing improved extension of the three component method in Y4R [7] and S4R. In addition, the total power differences between the measured data and the decomposition results over the oriented urban areas for patch A are listed in Table I. Although they are very small (less than 0.2%), the relative error order is G4U < Y4R < S4R.

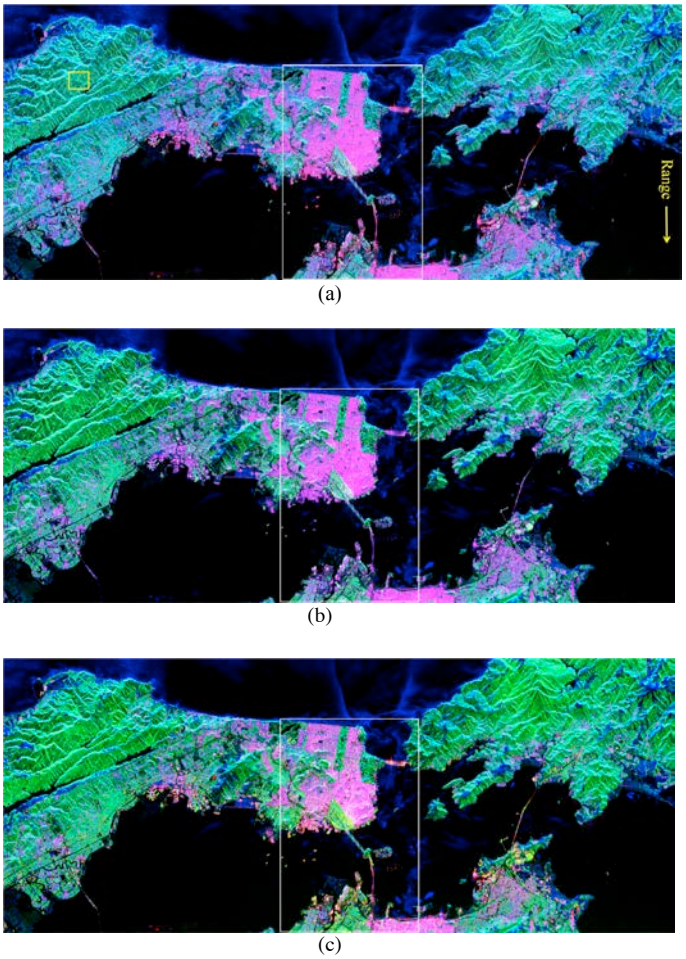

Fig. 3. Color-coded scattering power decomposition with Red (double bounce), Green (volume scattering), Blue (surface scattering). (a) G4U: New four-component decomposition with unitary transform coherency matrix and $T_{23} = 0$. The *HV* component is assigned to dihedral and dipole scattering. (b) S4R: four-component decomposition with Re{T_{23}} = 0 rotation. The *HV* component is assigned to dihedral and dipole scattering. (c) Y4R: Four-component decomposition with Re(T_{23}) = 0 rotation. The *HV* component is assigned only to dipole scattering.

The decomposition power contribution of vegetation areas in the San Francisco image are also shown in Table II, for yellow line box in Fig. 3, for quantitative comparison of the existing 4-component schemes *versus* the proposed 4-component scheme. It has been observed that the volume scattering components of the proposed methods are preserved and the surface scattering components of the present methods are increased as compared to the method Y4R [7] and S4R. The double bounce scattering components of present methods are decreased as compared to the methods Y4R [7] and S4R.

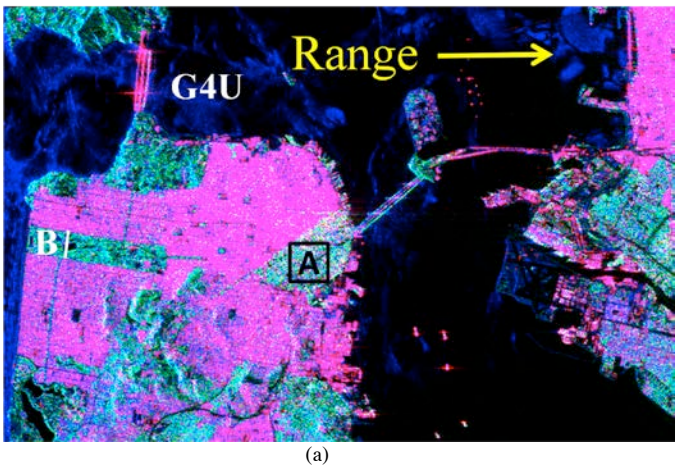

(a)

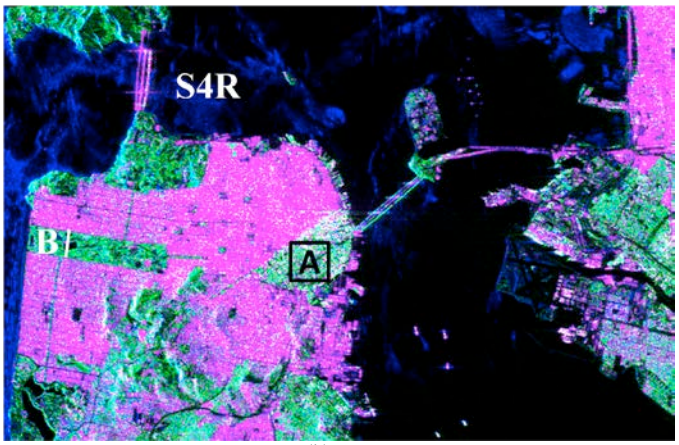

(b)

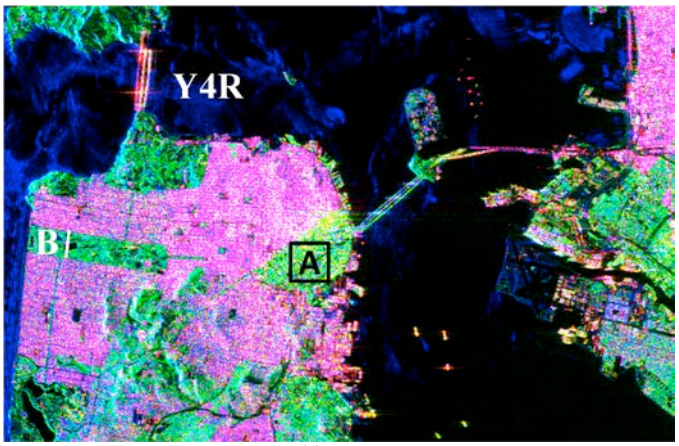

(c)

Fig. 4. Close-up view of white rectangular images in Fig.3. (a) G4U: New four-component decomposition with unitary transformed coherency matrix. (b) S4R: four-component decomposition with Re$\{T_{23}\} = 0$ rotation. The *HV* component is assigned to dihedral and dipole scattering. (c) Y4R: Four-component decomposition with Re$(T_{23}) = 0$ rotation.

TABLE I

DECOMPOSITION MEAN POWER STATISTICS OVER THE ORIENTED URBAN AREA FOR PATCH A (BLACK LINE BOX IN FIG. 4) IN SAN FRANCISCO IMAGES IN FIG. 4

Methods	P_s	P_d	P_v	P_c	*TP* from results	*TP* from data
S4R	0.415	0.444	0.432	0.117	1.408	1.405
G4U	0.406	0.450	0.432	0.117	1.405	1.405
Y4R	0.385	0.435	0.467	0.117	1.404	1.405

TABLE II

DECOMPOSITION MEAN POWER STATISTICS OVER THE VEGETATION AREA FOR YELLOW LINE BOX IN FIG.3

Methods	P_s	P_d	P_v	P_c	*TP* from results	*TP* from data
S4R	0.089	0.045	0.26	0.029	0.423	0.423
G4U	0.091	0.043	0.26	0.029	0.423	0.423
Y4R	0.089	0.045	0.26	0.029	0.423	0.423

In order to further examine the volume scattering result of the newly proposed method, the decomposition power profiles along a transect B in Fig. 4 (or white line in Fig. 5) over the forest, the POLO ground and the orthogonally oriented urban areas, respectively, are shown in Fig. 5. It has been found that the proposed method preserves the amount of the volume scattering in vegetation and POLO ground areas similar to the Y4R [7] and the S4R. Furthermore, statistics of whole image pixels processed by using the four volume scattering models are given in Table III.

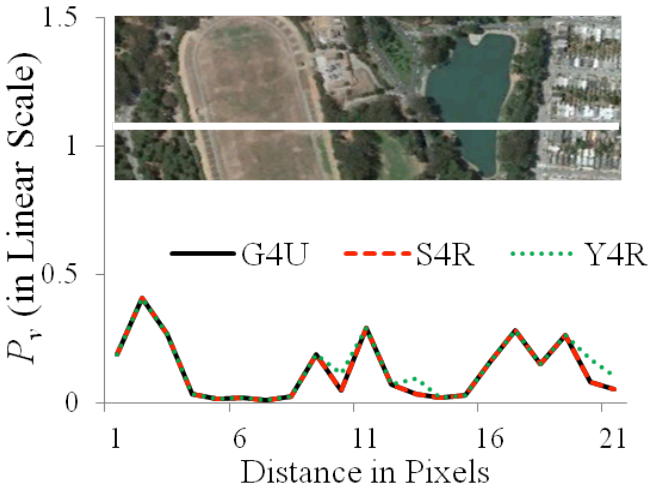

Fig. 5. Decomposition scattering power P_v profile along white line (same as white line B in Fig.4) for various targets

TABLE III
PROCESSED PIXEL STATISTICS OF P_v BY USING THE FOUR VOLUME SCATTERING MODELS AND BY THE POWER CONSTRAIN

Area/ Feature	POLSAR Data	P_s (%)	P_d (%)	P_v (%)	*Dominant Scattering*
Golden Color Box/ Vegetation Areas	Radarsat-2	31.1	4.8	59.7	Volume
	PALSAR	35.2	8.2	50.9	
Black Box /Urban Areas	Radarsat-2	30.6	62.7	5.6	Double bounce
	PALSAR	47.2	47.8	1.8	
White Box/ Airport Runway Areas	Radarsat-2	45.9	12.4	37.9	Surface
	PALSAR	47.4	10.2	37.8	

Proposed G4U method is also applied on fine beam mode (FQ9) quad polarization Radarsat-2 image (acquired on April 9, 2008) over the San Francisco with multi-look factors 6 in the range direction and 12 in the azimuth direction. A color-coded image of proposed G4U method results with Radarsat-2 data sets is shown in Fig. 6. A comparison of decomposition results with C- band and L-band POLSAR data has been investigated for vegetation (volume scattering dominant features), urban (double-bounce scattering dominant areas) and airport runway (surface scattering dominant) areas. The statistics of the scattering power contribution shifting from volume scattering (golden color box in Fig.6) at C-band to the surface and double bounce scattering in L-band in vegetation areas are shown in Table IV. Moreover, similar statistics for the change of single bounce (airport runway areas, white box in Fig.6) and double bounce (orthogonal urban areas, black box in Fig.6) at C-band to other scattering classes at L-band are shown in Table IV.

Fig. 6. A color-coded image of proposed G4U method results with Radarsat-2 data sets. RADARSAT-2 Data and Products © MacDonald, Dettwiler and Assocates Ltd., 2008 - All Rights Reserved.

Due to longer wavelength of L-band as compared to C-band and nearly 5.5^0 lower incident angle of the acquired PLASAR scene (23.5^0) than the angle of incidence of the acquired Radarsat-2 scene (29^0), L-band PLASAR scene reflects the surface and double bounce scattering more than C-band Radarsat-2 scene in vegetation areas. Moreover, it can be seen that the double bounce contribution is reduced by 14.9% at L-band PALSAR data as compared to C-band Radarsat-2 data. The surface scattering dominant areas show slightly higher contribution at L-band than C-band POLSAR data.

TABLE IV
SURFACE (P_s), DOUBLE BOUNCE (P_d) AND VOLUME (P_v) SCATTERING POWER COMPONENT CONTRIBUTION STATISTICS OF PROPOSED G4U METHOD FOR THE C-BAND AND L-BAND OVER THE VEGETATION AREAS (GOLDEN COLOR BOX IN FIG.6), URBAN AREAS (BLACK BOX IN FIG.6) AND AIRPORT RUNWAY AREAS (WHITE BOX IN FIG.6)

Models	Pixels processed by	Sin	Cos	Uniform	Oriented dihedral
Y4R	Model	283473	44605	623437	
	Power Constrain	2601	269	4079	-
S4R/ G4U	Model	245513	42442	590470	77422
	Power Constrain	835	76	2012	0

V. CONCLUSION

A new four-component scattering power decomposition scheme is presented in this paper. The element T_{23} of the measured rotated coherency matrix is completely eliminated by implementing of double unitary transformations. This four-component decomposition accounts for 7 parameters out of 7 independent polarimetric parameters included in the coherency matrix. Therefore, this method uses full polarimetric information in the decomposition. The double bounce component is enhanced over the urban areas. It was shown that this method yields accurate and/or similar decomposition images compared with those by the existing four-component decomposition [7], [8] resulting from the full utilization of polarimetric information.

ACKNOWLEDGMENT

The authors are grateful to JAXA for providing ALOS-PALSAR data sets. The authors would like to thank Prof. W.-M. Boerner, Professor Emeritus at the University of Illinois at Chicago for improving the manuscript. RADARSAT-2 Data has been downloaded from the RADARSAT-2 website.

REFERENCES

[1] J. S. Lee and T. Ainsworth, "The effect of orientation angle compensation on coherency matrix and polarimetric target decompositions," *IEEE Trans. Geosci. Remote Sens.*, vol. 49, no. 1, pp. 53-64, Jan. 2011.

[2] J. S. Lee and E. Pottier, Polarimetric radar imaging from basics to applications, CRC Press, 2009.

[3] A. Freeman and S. Durden, "A three-component scattering model for polarimetric SAR data," *IEEE Trans. Geosci. Remote Sens.*, vol. 36, no. 3, pp. 963-973, May 1998.

[4] Y. Yamaguchi, T. Moriyama, M. Ishido, and H. Yamada, "Four-component scattering model for polarimetric SAR image decomposition," *IEEE Trans. Geosci. Remote Sens.*, vol. 43, no. 8, pp. 1699-1706, Aug. 2005.

[5] Yajima, Y. Yamaguchi, R. Sato, H. Yamada, and W.-M. Boerner, "POLSAR image analysis of wetlands using a modified four-component scattering power decomposition," *IEEE Trans. Geosci. Remote Sens.*, vol. 46, no. 6, pp. 1667-1773, June 2008.

[6] W. An, Y. Cui, and J. Yang, "Three-component model-based decomposition for polarimetric SAR data," *IEEE Trans. Geosci. Remote Sens.*, vol. 48, no. 6, pp. 2732-2739, 2010.

[7] Y. Yamaguchi, A. Sato, W.-M. Boerner, R. Sato, and H. Yamada, "Four-component scattering power decomposition with rotation of

coherency matrix," *IEEE Trans. Geosci. Remote Sens.*, vol. 49, no. 6, pp. 2251-2258, June 2011.

[8] A. Sato, Y. Yamaguchi, G. Singh, and S.-E. Park, "Four-component scattering power decomposition with extended volume scattering model," *IEEE Geosci., Remete Sens. Lett.*, vol. 9, no. 2, pp. 166-170, Mar. 2012.

[9] M. Arii, J. J. van Zyl, and Y. Kim, "A general characterization for polarimetric scattering from vegetation canopies," *IEEE Trans. Geosci. Remote Sens.*, vol. 48, no. 9, pp. 3349-3357, Sep. 2010.

[10] M. Arii, J. J. van Zyl, and Y. J. Kim, "Adaptive model-based decomposition of polarimetric SAR covariance matrices," *IEEE Trans. Geosci. Remote Sens.*, vol. 49, no. 3, pp. 1104 – 1113, Mar. 2011.

[11] R. Touzi, "Target scattering decomposition in terms of roll-invariant target parameters," *IEEE Trans. Geosci. Remote Sens.*, vol. 45, pp. 73-84, Jan. 2007.

[12] J. J. Sharma, I. Hajnsek, K. P. Papathanassiou, A. Moreira, "Polarimetric decomposition over glacier ice using long- wavelength airborne PolSAR," *IEEE Trans. Geosci. Remote Sens.*, vol. 49, no. 1, pp. 519-535, January 2011.

[13] M. Shimada "Model-based polarimetric SAR calibration method using forest and surface scattering targets," *IEEE Trans. Geosci. Remote Sens.*, vol. 49, no. 5, pp. 1712–1733, May. 2011.

[14] J. J. Van Zyl, M. Arii, and Y. Kim, "Model-based decomposition of polarimetric SAR covariance matrices constrained for nonnegative eigenvalues," *IEEE Trans. Geosci. Remote Sens.*, vol. 49, no. 9, pp. 3452-3459, Sep 2011.

Gulab Singh (S'09–M'10) received his B.Sc. and M.Sc. degrees in physics from the Meerut University, Meerut, India in 1998 and 2000, respectively, and his M. Tech. degree in remote sensing from the Birla Institute of Technology, Ranchi, India in 2005 and his Ph.D. from Indian Institute of Technology Bombay, Mumbai, India in 2010. From 2005 to 2007, he was Research Fellow at Indian Institute of Technology Bombay, Mumbai, India, where he was involved in several research projects related to POL-SAR and In-SAR data analysis for snow and ice parameters retrieval. He is currently Post Doctoral Fellow at Graduate School of Science and Technology, Niigata University, Niigata, Japan. His current research interests include SAR data analysis, SAR polarimetry and SAR interferometry techniques development for earth and lunar surface parameters estimation.

Yoshio Yamaguchi (M'83-SM'94-F'02) received the B.E. degree in electronics engineering from Niigata University, Niigata, Japan, in 1976, and the M.E. and Dr. Eng. degrees from the Tokyo Institute of Technology, Tokyo, Japan, in 1978 and 1983, respectively. In 1978, he joined the Faculty of Engineering, Niigata University. From 1988 to 1989, he was a Research Associate at the University of Illinois at Chicago, Chicago. His interests are in the field of radar polarimetry, microwave sensing, and imaging.

Dr. Yamaguchi has served as Chair of IEEE Geoscience & Remote Sensing Society (GRSS) Japan Chapter (2002–2003), Chair of International Union of Radio Science Commision F Japanese Committee (URSI-F) Japan (2006–2011), Associate Editor for Asian affairs of GRSS Newsletter (2003–2007), and Technical Program Committee (TPC) Co-Chair of the 2011 IEEE International Geoscience and Remote Sensing Symposium (IGARSS). He is a Fellow of the Institute of Electronics, Information and Communication Engineers (IEICE), Japan, and a recipient of the 2008 IEEE GRSS Education Award.

Sang-Eun Park (S'05-M'07) received the B.S. and M.S. degrees in geophysics and Ph.D. degree in radar remote sensing and geophysics from the Seoul National University, Seoul, Korea, in 2000, 2002, and 2007 respectively. From 2007 to September 2009, he worked at the Radar Polarimetry Remote Sensing Group of the University of Rennes 1, Rennes, France, for a post-doctoral fellow on radar polarimetry. From October 2009 to January 2010, he was a project scientist in the Institute of Photogrammetry and Remote Sensing, Vienna University of Technology, Vienna, Austria. He is currently an Assistant Professor in the Graduate School of Science and Technology at Niigata University, Japan. His research interests include polarimetric SAR classification, forward and inverse modeling of microwave vegetation and surface backscattering, and investigation of multi-source data integration methodology.